sciendo

POLISH MARITIME RESEARCH 3 (127) 2025 Vol. 32; pp. 47-65
10.2478/pomr-2025-0035

Numerical Simulation Study of the Hydrodynamic Properties of a Floating Breakwater of Pontoons

Xiaofei Cheng [1]
Shimin Li [2 *]
Wei Xie [1]
Chenhan Xu [2]
Junnan Wang [2]
Tiaojian Xu [3]
[1] School of Civil and Ocean Engineering, Jiangsu Ocean University, Lianyungang 222005, China
[2] School of Ocean Engineering, Jiangsu Ocean University, Lianyungang 222005, China
[3] State Key Laboratory of Coastal and Offshore Engineering, Dalian University of Technology, Dalian 116024, China

* Corresponding author: *2022220311@jou.edu.cn (Shimin Li)*

ABSTRACT

To address the issue of insufficient wave dissipation capacity in standard floating breakwaters consisting of pontoons, this research proposes a combined floating breakwater with T-block connections. AQWA software is used to conduct numerical simulation studies on the dissipation characteristics of waves, and the reliability of the results is confirmed by integrating them with tests of a physical model. It is found that the transmission coefficient of the combined floating breakwater increases with the wave period. When the incident wave period T<6 s, increasing the relative height of the T-block improves the wave dissipation performance; when T>6 s, the effect is weakened; and at T=8 s, the change in height is basically unaffected. Increasing the relative width of the T-block is more significant in terms of the enhancement of the wave dissipation performance, whereas the height of the incident wave has a smaller effect on the transmission coefficient, and the transmission coefficient tends to increase with the increase of the wave height only in the case where T=8 s. The height of the incident wave has little effect on the transmission coefficient. The transmission coefficient increases with the wave height only when T=8 s; when the wave period is small (e.g. 4 s), the effect of wave elimination is enhanced by increasing the draught depth, and the draught does not have a significant effect on the wave dissipation performance when T>6 s. Compared with a typical floating pontoon breakwater with a single- and double-row arrangement, the combined floating pontoon breakwater has a better effect in terms of dissipating the waves, and its advantage is significant for a period T≤6 s, with a 44% increase in the maximum wave abatement compared to a single-row arrangement. In addition, the free-motion response is analysed to clarify the effects of different factors on the transverse and pendulum motion. This study provides an important reference for the design and application of floating pontoon breakwaters.

Keywords: Floating pontoon breakwater, AQWA, Numerical simulation, Wave dissipation characteristics, Motion response

INTRODUCTION

In recent years, with the development of the world economy, the shipping industry has undergone rapid growth. The numbers of ships in ports are increasing day by day, and breakwaters are constructed in each port to ensure the safety of docked ships and port facilities. However, typical seated breakwaters are costly and difficult to install, and maintenance work is not easy in the later stages. In this case, a special type of breakwater, called a floating breakwater, has become a new option. A floating breakwater is composed of a mooring system and floating body; the latter is mainly used to dissipate waves, while the former is used to fix the upper part of the floating body. Compared with a typical breakwater, a floating breakwater has a strong water quality exchange function, can prevent seawater pollution, and can be used in deep water; in addition, with an increase in the water depth, the project cost is reduced, with a greater water depth giving a more obvious cost advantage. It can be used with a soft soil seabed, with no need to carry out foundation treatment, and it can also be relocated, as it is rapidly constructed and easy to dismantle and relocate. The construction cycle is short, and a modular prefabrication approach can be used for on-site installation at sea. It causes only small amounts of environmental damage, does not inflict a great deal of damage on the marine geomorphology, and is conducive to the protection of the marine ecological environment [1,2]. Since the floating breakwater has such a simple installation process, is easy to maintain and has many other advantages, it has attracted attention from researchers in recent years.

In 1811, the first wooden floating breakwater was established in Plymouth harbor in Britain, and in 1976, a floating breakwater was built in in Fukuyama, Japan [3]. In the Moroccan port of Rabat, a box-type floating breakwater was built of reinforced concrete, which was 352 m long, 28 m wide, and weighed 13,000 tons [4]. In 2002, China's first floating breakwater was constructed in Lianyungang City, with a total length of 1,000 m, so that the Lianyungang Qitai Mountain, under originally windy and rough seas, could be turned into an area that would be available for marine aquaculture [5]. It can also be seen that the floating breakwater has a wide range of application prospects. Over the past 100 years, many scholars have conducted research on floating breakwaters in order to improve their wave dissipation performance. At the end of the last century, Sawaragi [6] proposed that floating breakwaters could be classified into four types, depending on the wave dissipation mechanism, as reflecting, reflecting, breaking wave, and friction breakwaters.

Most of the research on wave dissipation by floating breakwaters has involved physical modeling experiments and numerical simulation studies. Authors who have carried out physical modeling experiments include Chun-Yan Ji et al. [7], who proposed a new type of drum-type breakwater and conducted two-dimensional flume tests to show that this cylindrical floating breakwater yielded better wave dissipation performance than the traditional double floating box type breakwater. Chao [8] studied the wave dissipation of a rectangular box type of floating breakwater, and showed that the relative width of the square box, the relative draft depth and the initial tension of the anchor chain had an effect on the wave dissipation performance of the breakwater. Loukogeorgaki et al. [9, 10] carried out a three-dimensional physical modeling study of an inverted trapezoidal floating breakwater connected via a flexible structure to study the effect of waves on the breakwater structure and the wave dissipation performance. Li et al. [11] designed a new type of porous floating breakwater and carried out a physical modeling study of this device, and showed that this type of breakwater has a certain wave dissipation performance for short waves. Hou Yong [12] studied a unilateral box-type floating breakwater under the action of regular waves through physical modeling experiments to analyse the effects of the relative width, relative towing length of the anchor chain, and other factors on its wave dissipation performance, motion characteristics, and anchor chain force characteristics. Cheng et al. [13] explored the wave elimination characteristics of typical pontoons through physical modeling, and found that a floating breakwater composed of abandoned pontoons had a better wave elimination effect for incident waves with a wave period of about 4 s. Corsano et al. [14] conducted physical model experiments and reported that the mooring system is a critical component of floating breakwaters in terms of both wave attenuation and mooring forces. Compared to other mooring configurations, the vertical mooring method resulted in lower tension in the mooring lines. Christian [15] added vertical skirts to a typical rectangular floating breakwater, which resulted in a reduction of the transmission coefficient of the floating breakwater, but found that a vertical plate that was too deep could lead to an increase in the transmission coefficient.

Physical modeling experiments are subject to limitations arising from the site, the time and instrumentation required, experimental costs, and other factors, meaning that many aspects of the process are difficult to control. At the same time, professional numerical simulation software continues to advance with developments in computer science, and the use of numerical simulation technology for experimental research including physical modeling experiments to validate and supplement numerical simulation techniques has become a significant method of studying floating breakwaters. Headland [16] developed a time-domain analysis model and proposed that the anchor chain force of the mooring system could be better analysed by time-domain analysis. Chen et al. [17] used AQWA to conduct a numerical simulation study, and found that the addition of wing plates to both sides of a traditional floating square box could provide better wave dissipation in long-period waves. Cheng et al. [18] found numerical simulation that placing an airbag at a distance of 0.75 times the wavelength behind a pontoon-type floating breakwater could enhance its wave dissipation performance, which increased with longer wave periods.

Wang et al. [19] explored the potential of decommissioned ocean-going vessels as floating breakwaters and the application of gap resonance to wave dissipation through physical modeling experiments and numerical simulations using AQWA. Yin et al. [20] investigated the hydrodynamic characteristics of a box-type floating breakwater with restraining piles under the action of regular waves through experiments and 2D CFD numerical analysis, in order to ascertain the effects of different parameters on the hydrodynamic coefficients and longitudinal rocking angles. These authors also gave prediction equations for the hydrodynamic coefficients. In [21], the researchers conducted numerical simulations to compare the performance of circular and rectangular cross-section floating breakwaters under wave conditions. It was found that circular cross-section floating breakwaters generally outperformed rectangular ones across most wave frequency ranges, with lower transmission coefficients and more effective attenuation of wave energy. Zheng et al. [22] used AQWA software to numerically simulate the wave dissipation performance of an OWC (Oscillating water column)-perforated floating breakwater under irregular wave action. Mao et al. [23] analysed the wave loads on a floating breakwater with a curved layout based on three-dimensional potential flow theory, and the showed that a curved breakwater could effectively reduce the first-order and second-order wave forces on the floating breakwater structure, making the structure's profile loads under oblique waves consistent with those under cross-wave conditions.

In [24],the researchers employed the smoothed particle hydrodynamics (SPH) method to study the wave attenuation mechanisms of floating breakwaters. The results indicated that the vertical position of the horizontal plates and wave characteristics had a direct impact on energy dissipation and wave reflection mechanisms.Yuan et al. [25] employed the SPH method to simulate the performance of a quadruple-wing configuration (upper-wing, lower-wing, and four-wing arrangements) in floating breakwaters under both regular and irregular wave conditions, and showed that the four-wing configuration yielded optimal wave attenuation performance in irregular wave scenarios, with motion response operator amplitudes that were reduced by approximately 50% compared to non-winged models. Sun et al. [26] investigated the wave attenuation performance and dynamic response of kelp-integrated modular floating breakwaters through experimental and numerical simulations. Their study revealed that an increase in kelp length, a reduction in planting intervals, and higher numbers of rows could significantly enhance the long-wave attenuation capacity. Turbulent kinetic energy variations and vortex shedding mechanisms were identified as the dominant wave energy dissipation pathways. Guo et al. [27] investigated the effects of tight, loose and hybrid mooring systems on the hydrodynamic performance of floating breakwaters via numerical simulations based on SPH. The results showed that at low tide, a tight-tie mooring system had the lowest transmission coefficient but the largest mooring force, due to the restriction of structural motion and the enhancement of wave reflection and wave dissipation. The hybrid system had the second highest wave dissipation effect, and the mooring force was significantly reduced. At high tide, the tight system was still optimal for short-wave conditions, while the hybrid system had the lowest transmission coefficient for long-wave conditions, due to energy dissipation caused by structural inclination-induced wave climbing.

Numerous studies have been conducted to improve the wave attenuation performance of floating breakwaters. One effective approach involves the incorporation of submerged vertical structures, as exemplified by the following studies. Work by Ursell [28] proved that the placement of vertical plates in deep water can play a reflective role in regard to waves, and in particular that short waves greatly reduce the transmission coefficient. At the same time, it was shown that the installation of vertical plates as wave dissipation elements on floating breakwaters can not only deepen the local draught of breakwaters, but also improve the performance of wave dissipation of breakwaters. Neelaman [29] designed a T-type breakwater by combining the characteristics of horizontal and vertical plates, and showed that this structure yielded good wave dissipation performance in deep water areas. Gesraha [30] carried out physical modeling tests to explore the installation of a vertical version on both sides of the square box, finding that this could increase the additional mass of the floating body and that rise and sink damping improved the wave dissipation performance of the floating breakwater. For short, oblique waves, the transmission coefficient of this breakwater was higher than for a rectangular breakwater. Huang et al. [31] installed barrier plates with slots at the bottom of a square box floating breakwater to create vortex shedding through the slotted barrier, in order to dissipate energy and improve the wave dissipation performance of the breakwater. The hydrodynamic performance of rectangular floating breakwaters installed with vertical plates was investigated by He et al. [32] through physical modeling and experiments that systematically explored the effects of installation location, number of rows of the installation, plate porosity, and plate outreach height on the performance in terms of the wave protection and motion response of the breakwaters.

The present study focuses on a floating breakwater system composed of decommissioned pontoon vessels. Previous investigations have focused on standard single-pontoon floating breakwaters, and have revealed that structures constructed from individual decommissioned pontoons have an effective wave attenuation capacity only for waves with periods below 4 s. Building upon these findings, this study proposes a composite pontoon floating breakwater system that incorporates T-shaped blocks to enhance the wave attenuation performance of the decommissioned pontoon structures. The hydrodynamic performance of this composite pontoon breakwater is investigated through an integrated approach combining physical modeling and numerical simulation.

3D POTENTIAL FLOW THEORY

The study presented in this paper is based on the potential flow theory, a mathematical model for describing the motion of a fluid. This theory is based on the concept of a potential function, which represents the velocity field of a fluid as a gradient of a potential function. In the 3D potential flow theory, it is assumed that the fluid is spinless, viscous and incompressible. The fluid should satisfy the Laplace equation in the flow field:

$$\nabla^2\Phi = \frac{\partial^2\Phi}{\partial x^2} + \frac{\partial^2\Phi}{\partial y^2} + \frac{\partial^2\Phi}{\partial z^2} = 0 \quad (1)$$

where $\nabla = \left(\frac{\partial}{\partial x}, \frac{\partial}{\partial y}, \frac{\partial}{\partial z}\right)$ is the Laplace operator, and Φ is the total velocity potential in the flow field.

According to the principle of linear superposition, the velocity potential in a simple harmonic propagating wave in a flow field with a floating rigid body can be decomposed into three parts, as follows:

$$\Phi(\mathrm{x,y,z,t}) = \Phi_I + \Phi_D + \Phi_R \quad (2)$$

where Φ_0 is the incident form of the wave when it is not disturbed by the floating body; Φ_d is the diffraction potential generated by the motion of the wave around the floating body; and Φ_r is the radiation potential generated by the motion of the floating body when the wave goes around the floating body.

Solving the Laplace equation gives the velocity potential function, and the pressure distribution at each point in the flow field can then be obtained. To ensure the Laplace equation has a unique solution, a series of boundary conditions must be imposed to constrain the equation.

Seafloor boundary conditions

At a finite depth of the seafloor, where the seafloor is a fixed boundary, the fluid has only tangential velocity with respect to the fixed boundary, and the velocity potential of its normal phase is zero, the following conditions are satisfied:

$$\frac{\partial \Phi_D}{\partial z} = 0, \quad z = -d \tag{3}$$

where d is the water depth.

Free liquid surface kinematic boundary conditions

At the surface of a body of water that is at rest, the velocity potential is constrained by the nonlinear kinematic boundary conditions, as follows:

$$\frac{\partial \eta}{\partial t} = \frac{\partial \Phi}{\partial z} - \frac{\partial \Phi}{\partial x}\frac{\partial \eta}{\partial x} - \frac{\partial \Phi}{\partial y}\frac{\partial \eta}{\partial y} \tag{4}$$

Free-surface kinetic boundary conditions

At the surface of still water, the velocity potential satisfies the nonlinear kinetic boundary condition, which is obtained from Bernoulli's equation:

$$\frac{\partial \Phi}{\partial t} + \frac{1}{2}|\nabla\Phi|^2 + g\eta = 0 \tag{5}$$

In Eqs. (4) and (5), g is the acceleration of gravity; η is the height of the free liquid surface above the hydrostatic surface; and t is time.

Boundary conditions at the surface of the object

For an impermeable solid wall surface, the normal velocity at any point on the surface must equal the normal velocity of the fluid particles in immediate contact with that point.

$$\frac{\partial \Phi}{\partial n} = U \cdot n \tag{6}$$

where U is the velocity of the motion of the mass, and n is the normal vector of the motion of the floating body.

Boundary conditions at infinity

At the surface of a free liquid, wave radiation occurs at the free surface at infinity, which must satisfy the following conditions in three-dimensional problems:

$$\lim_{r\to\infty} \sqrt{r}\left(\frac{\partial \Phi}{\partial t} + c\frac{\partial \Phi}{\partial r}\right) = 0 \tag{7}$$

where c is the wave propagation velocity.

The basic equations of the 3D potential flow theory are the continuity equation and the potential flow equation. The continuity equation describes the conservation of mass of the fluid, which specifies that the mass of the fluid must remain constant at any moment. The potential flow equation describes the motion of the velocity field, and shows that the velocity field is determined by the gradient of a scalar potential function.

NUMERICAL MODEL

DESIGN AND PROPOSAL FOR A COMBINED FLOATING BREAKWATER

A pontoon is an unpowered, rectangular, flat-bottomed watercraft that is normally tethered to a beach via anchor chains or mooring rails, and which acts as a platform for loading and unloading cargo, or for people boarding and disembarking a vessel. Researchers [13] have studied the use of a floating breakwater composed of standard pontoons, and have shown that this breakwater has very good wave elimination performance for short waves. A physical modeling study of a typical pontoon floating breakwater presented by these authors proved that the typical pontoon square wave breakwater had a certain wave elimination effect for waves with period T=4s. However, as the wave period increases, the wave dissipation capability of an ordinary floating pontoon breakwater drops substantially. To meet the current engineering demands of the port and increase the wave dissipation capacity of the breakwater, a floating breakwater made of composed pontoons is constructed here by combining a large number of the abandoned pontoons stacked up in the harbour.

According to the *Steel Inland Waterway Ship Construction Code* produced by the China Classification Society [33], the primary scale ratio for a pontoon should comply with the following requirements: L/D≤45, B/D≤7. The main constituent of the proposed combined pontoon breakwater is a common pontoon in the harbour with dimensions of 40×10×3 m. Only the main part of the pontoon body is considered here, in order to simplify the research, and the pontoon's superstructure is omitted from the modeling process. Only the major section of the hull is retained.

A prefabricated T-block is used as a link between each pair of pontoons. This T-block is a reinforced concrete construction that can be manufactured in a variety of sizes. Six cast iron columns measuring 0.4 m in diameter and 0.6 m in height are installed 0.3 m from each side of the pontoon's upper deck, and the two sides of the T-type wing boards are fitted with cast iron columns corresponding to the port side of the pontoon's deck to enable linking with the pontoon. Fig. 1 shows how two or more pontoons can be joined using T-blocks to construct a combined pontoon floating breakwater.

The model considered in this paper is established by using a fixed Cartesian coordinate system, with the XY plane as the still water surface, the Z-axis perpendicular to the XY plane, and upwards as the positive direction. This study mainly investigates the wave dissipation characteristics and motion response of a floating square wave embankment made of pontoons with different combinations of T-blocks under the action of regular waves of different draft depths and periods.

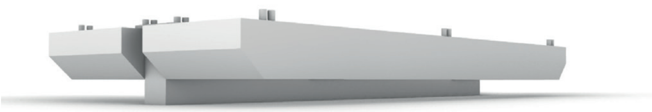

Fig. 1. Pontoon used to create a floating breakwater

The parameters involved in the numerical simulation of this paper are illustrated in Table 1. Table 2 shows the model grouping scheme.

Table 1. Parameters and their symbols

Parameter	Notation
Water depth (m)	h
Wave height (m)	H
Wave period (s)	T
Draft of pontoon (m)	d
Height of pontoon (m)	D
Width of pontoon (m)	B
Width of T-block (m)	b
Height of T-block (m)	S
Length of T-block (m)	l

Table 2. Model grouping scheme

Model	Relative width of T-block b/B	Relative height of T-block S/D
Different heights	0.1	1.00
	0.1	1.17
	0.1	1.33
	0.1	1.50
Different widths	0.1	1.50
	0.2	1.50
	0.3	1.50
	0.4	1.50

DESIGN OF THE MOORING SYSTEM

The mooring system has an important effect on a floating breakwater, since different mooring methods have an important effect on its motion response. The main mooring methods for a floating breakwater can be divided into two types: anchor chain mooring, and tension leg mooring. In this paper, the working conditions are as follows: the simulated sea depth is 20 m, and the mooring system is based on anchor chain mooring, using an Ø78 AM2 anchor chain +125t anchor block. The arrangement of the anchor chain and block is shown in Fig. 2.

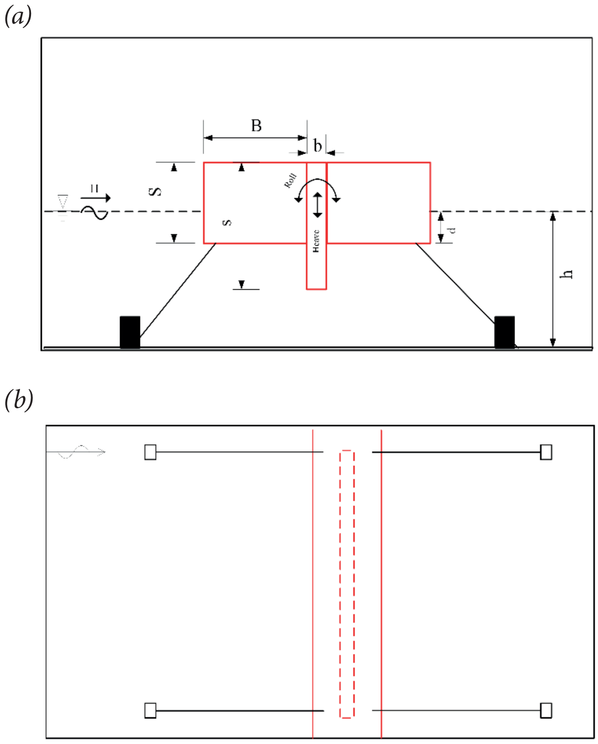

Fig. 2. Schematic diagram of mooring method: (a) elevation; (b) plan view

NUMERICAL SIMULATION OF WORKING CONDITIONS

In this paper, the numerical simulation assumes seawater with a density of 1.025 kg/m^3, and a gravitational acceleration of 9.8062 m/s^2. To investigate the effects of different draft depths and wave parameters on the wave attenuation performance and motion response of the combined pontoon floating breakwater, the experimental conditions were designed as shown in Table 3.

Table 3. Summary of experimental conditions

Parameter	Value
Experimental water depth *h*	20 m
Pontoon draft depth *d*	1.0, 1.5, 2.0 m
Wave period *T*	4, 5, 6, 7, 8 s
Wave height H	1.0, 1.5, 2.0, 2.5, 3.0 m

PHYSICAL MODELING EXPERIMENTS AND VALIDATION OF THE NUMERICAL SIMULATION

EXPERIMENTAL STUDIES OF PHYSICAL MODELS

Laboratory equipment and measuring instruments

The experiment was carried out in the wave tank at the Ocean Engineering Technology Research Center of Jiangsu Ocean University, which is 70 m long, 1.5 m wide and 1.8 m high. The tank has a push-plate type irregular wave maker (Fig. 3), which is automatically controlled by a computer to generate the required simulated wave elements.

Fig. 3. Experimental flume for wind and wave currents at Jiangsu Ocean University

This system can generate regular waves and irregular waves of different spectral types, as required. In order to eliminate multiple reflections of waves in the flume test, a secondary reflection absorption device is installed on the wave generating plate. The suction-type wind generation system consists of a variable frequency motor and an air duct, and a motor is installed at the end of the flume. Wave dissipation facilities are installed at both ends of the flume, and a connecting pipe is provided at the side of the flume to keep the water level on both sides of the model consistent during the test. The wave height is measured with a capacitive wave height meter (Fig. 4), which is connected to the computer via a collection card to automatically monitor and store the wave height, peak height and wave period (Fig. 5).

Fig. 4. Capacitive wave height meter

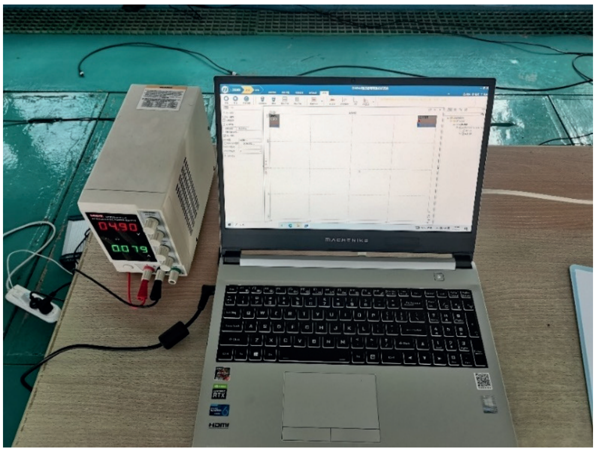

Fig. 5. Wave height acquisition system

All of the above instruments are computer-controlled and equipped with comprehensive data analysis and processing software. The instruments used for measuring wave height were strictly tested and calibrated before the test, and their performance was found to be reliable; in addition, during the test period, the wave height meter was regularly tested and calibrated.

The present experiment employed a normal model conforming to the Froude similarity criterion, with the structural cross-sections designed to meet geometric similarity requirements. The main scale relationships are as follows:

$$\lambda = \lambda_h = \frac{l_p}{l_m} = \frac{h_p}{h_m} \tag{8}$$

$$\lambda_w = \lambda^3 \tag{9}$$

$$\lambda_t = \lambda_T = \lambda^{\frac{1}{2}} \tag{10}$$

$$\lambda_L = \lambda_H = \lambda_h \tag{11}$$

where λ is the plane geometry scale; λ_h is the vertical geometric scale; l_p is the prototype length; l_m is the model length; h_p is the prototype vertical geometric scale; h_m is the model vertical geometric scale; λ_w is the weight scale; λ_t is the time scale; λ_T is the wave period scale; λ_L is the wavelength scale; and λ_H is the wave height scale.

Taking into account the constraints of the experimental facilities and site conditions, and following the model similarity principles described above, the main scale ratios for this experiment were established. Detailed values are provided in Table 4.

Table 4. Main scales for the model tests

Geometric scale λ	Time scale λ_t	Wavelength scale λ_L	Wave height scale λ_H	Wave period ruler λ_T	Weight scale λ_w
40	6.32	40	40	6.32	64000

Table 5. Dimensions of the pontoon models

Number	L (cm)	B (cm)	D (cm)
D1	100.0	25.0	7.50
T1	92	2.5	11.25
T2	92	5.0	11.25
T3	92	7.5	11.25
T4	92	10.0	11.25

The pontoon model was created using plexiglass as a raw material. According to the requirements of the physical model test of the floating structure, the model was shape was scaled geometrically to satisfy the Froude similarity criterion, while also ensuring geometric, center-of-gravity, and mass moment of inertia similarity. The simulation error in the centre of gravity should not be greater than ±1.0 mm, and the simulation error in the weight should not be greater than ±0.5%. The actual dimensions of the model components are shown in Table 5.

Mooring system

The mooring cable was simulated as a chain (Fig. 6), with four mooring holes set at the bottom of the pontoon. The anchoring method was based on both parallel anchoring and cross anchoring, where one end of the cable was connected to the pontoon model through the mooring holes, and the other end was fixed to the bottom of the tank. The distance of the anchor block from the pontoon was L_d=1.825 m. The anchoring method is illustrated in Fig. 7.

Fig. 6. Experimental anchor chain

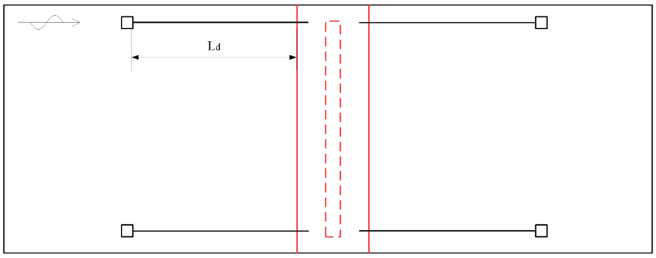

Fig. 7. Plan showing the anchor layout

Wave simulation

Regular waves were used in the experiment. The target significant wave height and period were input into the computer for wave generation, and repeated calibrations were performed to ensure that the wave height and period met the experimental requirements. For each test case, 15 waves were generated, which was sufficient to meet the experimental objectives while minimizing the influence of reflected waves. The specific wave elements are shown in Table 6.

Table 6. Regular Wave Parameters: Prototype vs. Model

Prototype value			Model value		
Water depth (m)	Wave height (m)	Period (s)	Water depth (cm)	Wave height (cm)	Period (s)
20	1.0	4.0	50	2.5	0.63
		5.0			0.79
		6.0			0.95
		7.0			1.11
		8.0			1.27
20	1.5	4.0	50	3.8	0.63
		5.0			0.79
		6.0			0.95
		7.0			1.11
		8.0			1.27
20	2.0	4.0	50	5.0	0.63
		5.0			0.79
		6.0			0.95
		7.0			1.11
		8.0			1.27
20	2.5	4.0	50	6.3	0.63
		5.0			0.79
		6.0			0.95
		7.0			1.11
		8.0			1.27
20	3.0	4.0	50	7.5	0.63
		5.0			0.79
		6.0			0.95
		7.0			1.11
		8.0			1.27

EXPERIMENTAL RESULTS

For the experiment with parallel mooring, the main scale of the pontoon remained the same, but the water depth was 0.5 m, the barge draught was 3.75 cm, the height of the T-block was 11.25 cm, and the width was set to values of 2.5, 5.0, 6.3, 7.5, and 10 cm. These physical modeling experiments were primarily carried out to analyse and study the impact of different T-block widths on the wave dissipation characteristics of the combined barge breakwater. Relative widths of b/B = 0.1, 0.2, 0.3, and 0.4 were considered as working conditions for the physical modeling experiments.

The configuration of the test site is depicted in Fig. 8. Two wave height test points were placed in front of the breakwater, and three wave height measurement stations were located behind it. For regular waves, the average wave height was used. Wave height meters W2 and W3 were 200 cm away from the breakwater. The distance between W1 and W2 was 25 cm, and these were used to measure the incident wave height. The distances between W3, W4, and W5 were also 25 cm, and these were used to determine the height of the transmitted wave behind the breakwater.

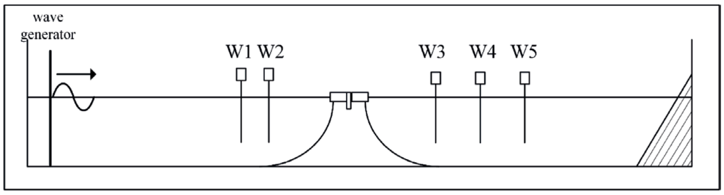

Fig. 8. Experimental layout of the combined floating breakwater physical model

According to the wave theory [34], when a wave encounters an obstacle during its propagation, a wave is generated in the opposite direction of the incident wave, a phenomenon known as wave reflection. If the reflecting surface is an ideal, smooth plane, the wave is completely reflected back to the original water, a phenomenon called complete reflection. However, in reality, the reflecting surface of the floating breakwater is not an ideal smooth and flat plane, meaning that the wave cannot be completely reflected in the process of propagation, and part of the wave will be transmitted or bypassed through the breakwater. In addition, friction with the surface of the breakwater will occur due to breaking of the wave, which will consume some of the energy, and only part of the wave will be reflected. In order to study the wave dissipation performance of the proposed floating breakwater, the transmittance coefficient K_t is introduced to evaluate the effect of wave elimination by the breakwater. The smaller the value of the transmittance coefficient K_t, the more wave energy is consumed and reflected by the breakwater, and the better the effect of wave elimination. Conversely, the larger the value of K_t, the worse the effect of wave elimination. The transmission coefficient can be calculated based on the ratio of the wave height behind the breakwater to the incident wave height.

$$K_t = \frac{H_t}{H_i} \tag{12}$$

where H_t is the wave height behind the breakwater, and H_i is the incident wave height.

The experiment was repeated in three groups, and the results were averaged. Fig. 9 shows a diagram of the experimental setup, and the results for the transmission coefficient are shown in Table 7.

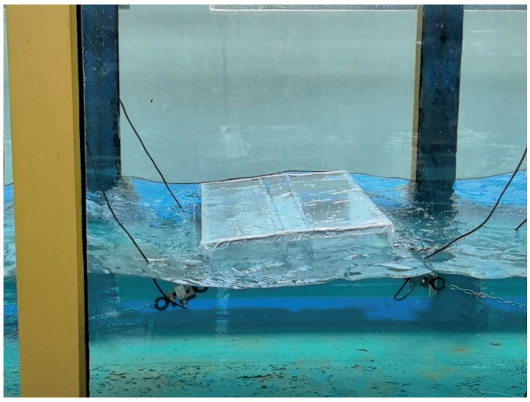

Fig. 9. Photograph of the experiment

Table 7. Effect of the relative width of the T-block on the transmission coefficient

Relative width	T \ H	1.0 m	1.5 m	2.0 m	2.5 m	3.0 m
b/B=0.1	4.0 s	0.35	0.35	0.34	0.34	0.36
	5.0 s	0.50	0.51	0.51	0.5	0.52
	6.0 s	0.67	0.68	0.69	0.69	0.7
	7.0 s	0.74	0.74	0.73	0.76	0.78
	8.0 s	0.78	0.78	0.77	0.8	0.83
b/B=0.2	4.0 s	0.28	0.28	0.29	0.28	0.28
	5.0 s	0.45	0.45	0.46	0.46	0.45
	6.0 s	0.64	0.65	0.66	0.64	0.67
	7.0 s	0.72	0.72	0.74	0.73	0.75
	8.0 s	0.76	0.74	0.73	0.72	0.78
b/B=0.3	4.0 s	0.24	0.25	0.26	0.26	0.25
	5.0 s	0.39	0.39	0.4	0.41	0.41
	6.0 s	0.57	0.6	0.63	0.61	0.6
	7.0 s	0.69	0.7	0.71	0.7	0.74
	8.0 s	0.76	0.79	0.8	0.83	0.85
b/B=0.4	4.0 s	0.20	0.19	0.19	0.2	0.19
	5.0 s	0.33	0.33	0.34	0.33	0.35
	6.0 s	0.54	0.54	0.53	0.55	0.56
	7.0 s	0.70	0.71	0.71	0.71	0.71
	8.0 s	0.76	0.77	0.79	0.82	0.84

Fig. 10 shows the results for the breakwater transmission coefficient with a change in the period of the incident wave for a combined pontoon floating breakwater formed by combining T-blocks with different widths, with the main body of the pontoon remaining unchanged and an incident wave height of 1 m. In this figure, the horizontal axis represents the period and the vertical axis represents the transmission coefficient.

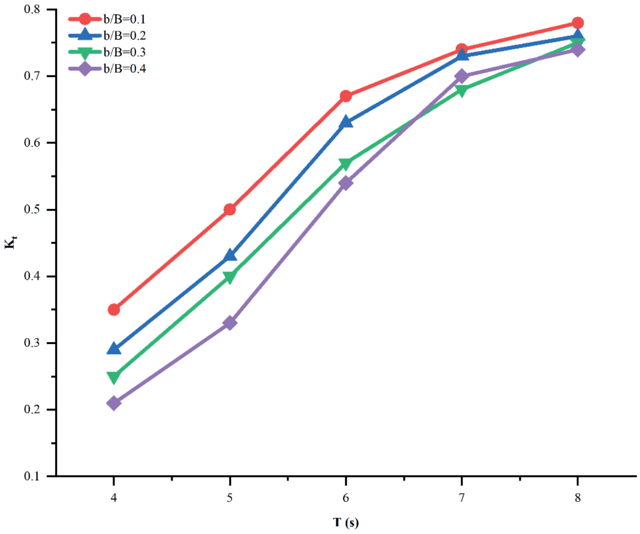

Fig. 10. Variation in the transmission coefficient with wave period (relative width) for a floating breakwater of combined pontoons

From Fig. 10, it can be seen that the breakwater transmission coefficient increases with the incident wave period, and its value ranges between 0.20 and 0.78. At the same time, the transmission coefficient tends to decrease as the relative width of the T-block increases. When the ratio b/B is 0.4 and the wave period is 4 s, the transmission coefficient is as low as 0.2, and under these conditions, the wave elimination effect can reach 80%. When the period is less than 7 s, the transmission coefficient of the combined floating breakwater decreases significantly with an increase in the width of the T-block, whereas when T=5 s, an increase in the width of the T-block has the greatest effect on the transmission coefficient, and the projection coefficient decreases by 0.17. When T=4 s, the transmission coefficient decreases by 0.14, but when the period is increased further and the wavelength becomes longer, the gain in wave dissipation induced by the increase in the relative width of the T-block decreases gradually, and the effect of wave elimination can reach 80% under this condition. When the period reaches 8 s, changes in the transmission coefficients of the four models are no longer obvious.

The four graphs in Fig. 11 illustrate the variation in the transmission coefficient with the period of the incident wave for different working conditions, with wave heights of 1, 1.5, 2, 2.5, and 3 m, respectively, using T-blocks of different widths. In these plots, the horizontal axis represents the period, and the vertical axis represents the transmission coefficient. The trends in the transmission coefficient curves are fairly similar for different wave heights. When the period is less than 7 s, the spacing between the curves is relatively narrow, indicating that a change in wave height does not have a significant effect on the transmission coefficient, whereas when the period is greater than 7 s, the transmission coefficient increases slightly with an increase in wave height. Overall, the values of the transmission coefficients corresponding to the same period do not change much when the wave height increases from 1 m to 3 m, despite the relatively large increase in wave height.

NUMERICAL SIMULATION STUDIES

Numerical simulation methods

In order to further study the wave dissipation performance of the proposed breakwater at its actual size, a numerical simulation experiment was carried out using ANSYS AQWA software to model the combined pontoon floating breakwater. This numerical simulation study was carried out using ANSYS version 2023R1. The model was first constructed by inputting the key coordinates or profile lines for the model with the help of DM software in Workbench. After the model had been constructed and validated to check for flaws, it was imported into the HD module to finish configuring the working conditions for the numerical simulation. In AQWA, the mesh size is closely related to the maximum allowable wave frequency in the simulation and the computational efficiency of the software. Based on the actual experimental conditions, the maximum mesh size for the model in this study was set to 0.5 m, with a mesh tolerance of 0.1 m. After defining the mesh parameters, the hydrodynamic diffraction module's meshing function was used to generate the computational

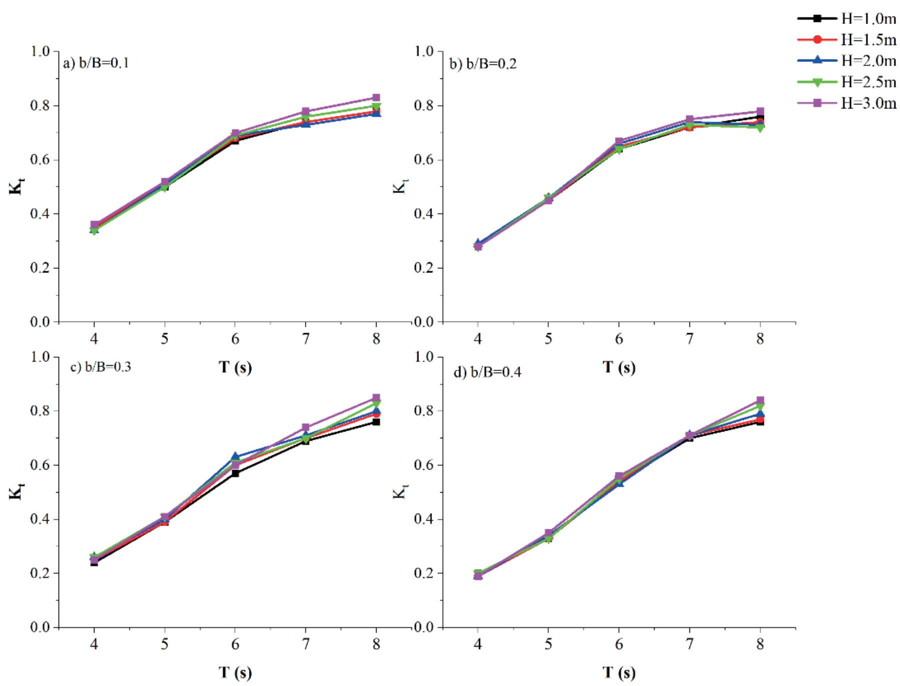

Fig. 11. Variation in the transmission coefficient with period for different wave heights

mesh for the model. The mesh generation is shown in Figure 12.

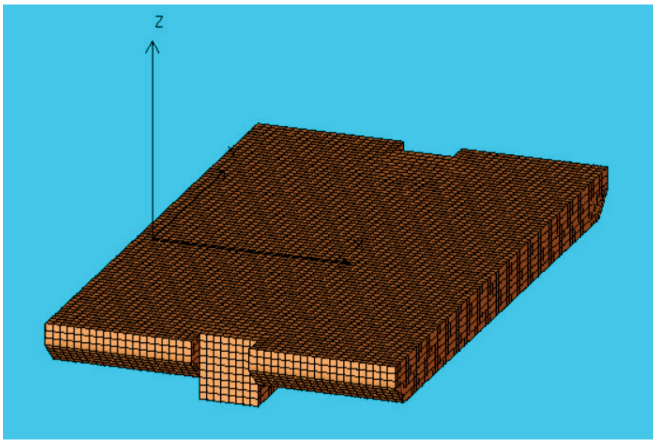

Fig. 12. Diagram showing the model meshing

After the numerical simulation was complete, the *.uss file containing the calculation results was read using Wave Contours in AQWA GS to obtain the wave map. By studying the wave cloud map, the change curve for wave amplitude could be retrieved, and the wave height behind the breakwater could be calculated, which serves as the foundation for the transmission coefficient.

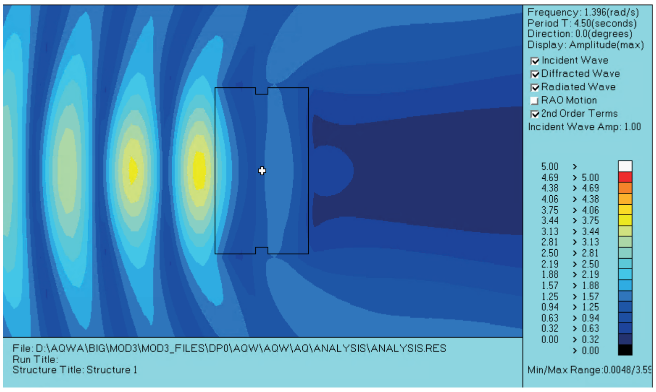

Fig. 13. Wave cloud diagram

Fig. 13 shows a wave cloud diagram for the model with relative width b/B=0.3, incident wave forward incidence, wave height H=1 m, and period T=4.5s. Fig. 14 shows the curve for the wave amplitude extracted from the centre of the model with a change in the X coordinate. It can be observed from the figure that the wave amplitude in front of the breakwater exceeds that of the incident wave. This phenomenon is attributed to wave reflection induced by the breakwater, leading to the superposition of the reflected and incident waves. Figs. 13 and 14 show that the wave amplitude decreases significantly behind the floating breakwater, indicating that the proposed combination pontoon floating breakwater has a positive effect on wave elimination.

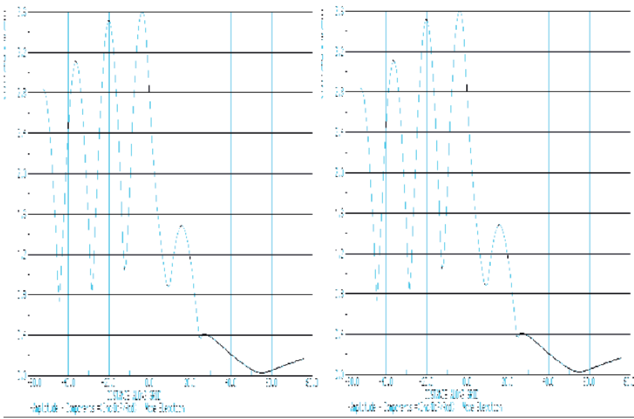

Fig. 14. Changes in wave amplitude with distance

In regular wave calculations, the averaging method is applied to calculate the post-dike wave height as follows:

$$H_t = \frac{\Sigma\eta(x,y)}{n} \tag{13}$$

This approach to the calculation involves taking the average value after counting the wave surface height η(x,y) of the points in the same region behind the floating breakwater, where n is the number of points taken in the rectangular area. To determine the transmission coefficient, five points are considered at distances of 10 to 20 m from the breakwater, and the average value is used to compute the wave height behind the breakwater using the formula given above.

Validation of the numerical simulation

1) Verification of the transmission coefficient

To verify the accuracy of the numerical simulation results, a combined pontoon floating breakwater with a relative width of b/B=0.3 was considered. Numerical simulations were performed under conditions with a wave height of 1 m and draught of 1.5 m, and the results were compared and validated against the results from the physical model experiments.

Fig. 15 shows the results from both the physical experiments and the numerical simulations with AQWA software for the combined pontoon floating breakwater with a relative width of b/B=0.3.

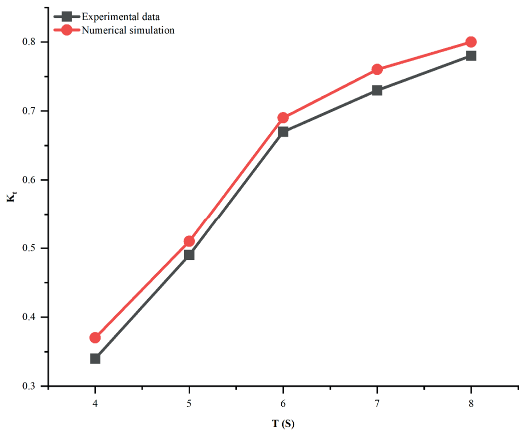

Fig. 15. Validation of the numerical results

From the figure, it can be seen that the transmittance coefficients obtained from both the experimental and numerical models tend to grow as the period of the incoming wave increases, and that the patterns of the changes are comparable. However, the numerical simulation produced somewhat better results than physical modeling, with an inaccuracy of roughly 3–6%. This minimal error range indicates that the results from the numerical simulation are reliable and that this experimental setup can be studied using numerical simulation.

Due to technical constraints arising from the experimental facilities and measurement equipment, measured data on motion amplitudes could not be obtained in the physical model tests. To address this limitation, a numerical model was established using AQWA software for the floating breakwater physical experiment described in reference [12], and a comparative validation was carried out against the experimental results from this prior study. The test protocol given in [12] has been replicated multiple times, demonstrating the high reliability and representativeness of its datasets. This established methodology provides a credible benchmark reference for validating the numerical model developed in this research. The validation model considered here was the experimental model numbered CASE4 in [12]. The size of rectangular box-type floating breakwater was 44×30×18 cm, and the mooring used was a parallel configuration, as illustrated in Fig. 16.

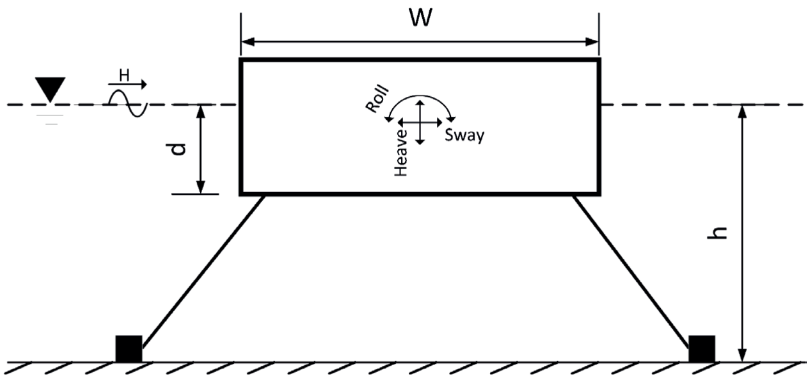

Fig. 16. Schematic diagram showing the anchoring method

In the numerical simulation experiments, the set of regular waves had the following parameters: the wave height H was 7 cm, and the wave period T was set to 0.70, 0.73, 0.81, 0.91, 1.10, 1.28, 1.46, and 1.55s, giving a total of eight different wave periods.

Fig. 17 compares the numerical simulation results recorded in this study against the experimental results from [12]. From Fig. 17, it is clear that the projection coefficients obtained with the two methods show the same pattern of variation with the period, with a maximum error of 7%, indicating that this numerical simulation can reflect the actual situation to some extent.

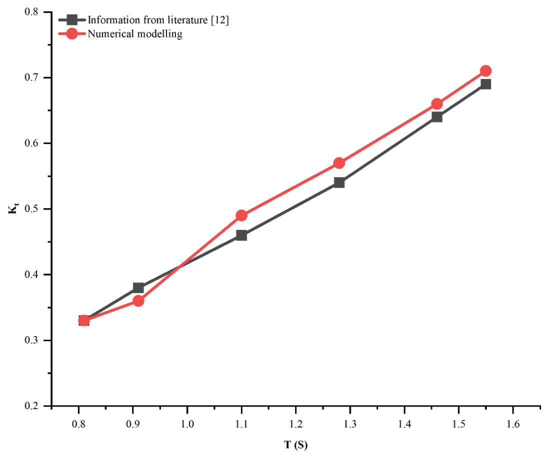

Fig. 17. Verification of the transmission coefficient

2) Motion response verification

The motion response amplitudes in roll and heave were obtained during the experiment, and a non-dimensionalization process was conducted to derive the corresponding Response Amplitude Operators (RAO). The specific formula is given in Eq. (14).

$$RAO = \frac{\text{Amplitude of motion}}{\text{Incident wave height}} \quad (14)$$

Fig. 18 shows a comparison of the transverse RAOs. In this graph, the vertical axis indicates the transverse roll RAO, while the horizontal axis represents the W/L ratio, i.e. the width of the model divided by the wavelength of the incoming wave. The numerical simulation results for the transverse roll RAO and the experimental results for the physical model in [12] show a high degree of similarity in terms of their behaviour: both first undergo a decreasing trend, then increase, and then decrease again, with an overall gradual increase in W/L. It is worth mentioning that the numerical simulations produce larger values than physical model experiments.

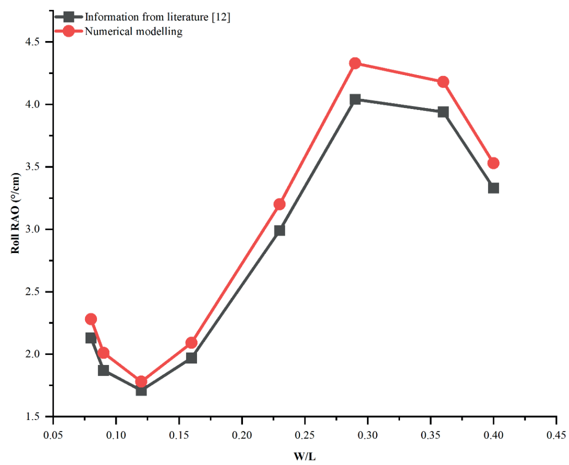

Fig. 18. Comparison of RAO results for roll

Figure 19 presents a comparison of the heave RAOs. In the figure, the vertical axis represents the heave RAO, while the horizontal axis denotes the width -to- wavelength ratio (W/L). The numerical simulation results show a similar trend to the physical model tests, with the heave RAO increasing as W/L increases.However, the numerical simulation results are slightly larger, with an error within 10%.

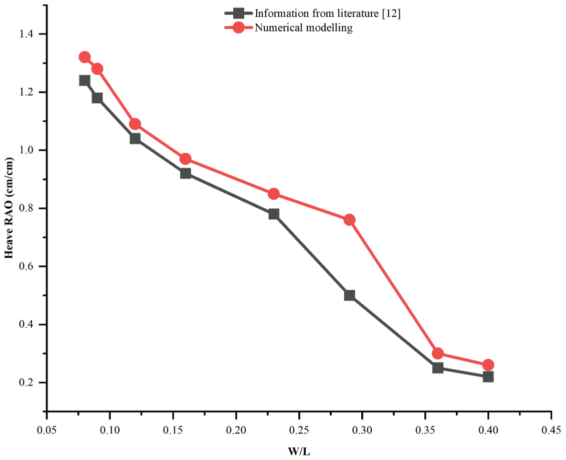

Fig. 19. Comparison of RAO results for heave

In summary, our numerical simulation yields higher values than the physical model for the amplitude of motion. The reason for this is that when the wave moves in the experimental process with the physical model, it produces friction with the model, which inevitably causes a certain amount of energy loss; in the numerical simulation, however, the friction loss is ignored, resulting in values that are larger than those obtained from the physical model experiments. Nonetheless, the error between the two outcomes is less than 10%, and the curves follow the same trend. Based on this finding, it is possible to conclude that the numerical simulation performed using AQWA can accurately simulate the motion response of the model, and that the simulation results have a high level of reliability and validity, meaning that they can be used as an important reference for other research and practical applications and provide strong data support and theoretical support for future work.

NUMERICAL SIMULATION RESULTS

INFLUENCE OF T-BLOCK HEIGHT ON WAVE DISSIPATION PROPERTIES

Fig. 20 depicts the results for the transmission coefficient of the breakwater with variation in the period of the incident wave, under conditions where the main body of the pontoon remains unchanged, the width of the T-block is 1 m, the height of the incident wave is 1 m, and a combination of T-blocks with different relative heights is used to form a floating breakwater made from pontoons. The horizontal axis shows the time, while the vertical axis represents the transmission coefficient.

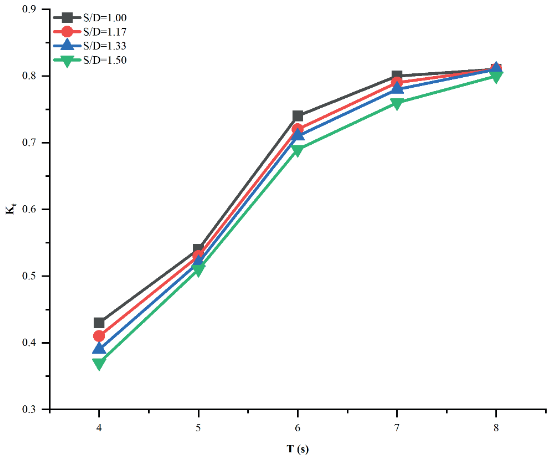

Fig. 20. Variation in the transmission coefficient with wave period for the combined pontoon floating breakwater (T-blocks with varying relative heights)

Fig. 20 shows that the transmittance coefficients of the four models rise as the wave period increases, and that when the period is shorter than 6s, increasing the relative height of the T-block improves the breakwater's wave dissipation performance. When T=4s, the transmittance coefficient for S/D=1.00 is 0.41, while that for S/D=1/50 is 0.36, meaning that the wave dissipation performance is marginally enhanced. When the period is longer than 6 s, there is very little change in the transmission coefficient, indicating that the effect of wave elimination is gradually diminished as the height of the T-block increases. When the period T is equal to 8s, a change in the height of the T-block has little influence on the transmission coefficient. This is because a wave with a short period has a limited wavelength and the majority of the energy is concentrated underwater. Increasing the height of the T-block improves the breakwater's relative draft, allowing it to better block the wave energy below the water's surface, thus limiting wave transmission through the breakwater. However, as the wave period increases, the wavelength grows longer, the wave speed slows, and the influence of the T-block's height diminishes.

INFLUENCE OF T-BLOCK WIDTH ON WAVE DISSIPATION PROPERTIES

Fig. 21 depicts the variation in the transmission coefficient for the breakwater with a change in the period of the incident wave, under working conditions where the main body of the pontoon remains unchanged, the height of the T-block is 4.5 m, the height of the incident wave is 1 m, and a combination of T-blocks with different relative widths is used to form the breakwater. The horizontal axis in the diagram shows the period, while the vertical axis represents the transmission coefficient.

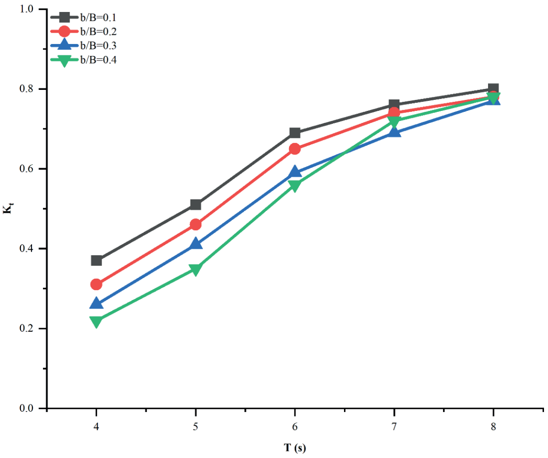

Fig. 21. Variation in the transmission coefficient with wave period for a combined pontoon floating breakwater (T-blocks with varying relative widths)

From Fig. 21, it can be seen that the transmission coefficient of the breakwater increases with the period of the incident wave, which ranges between 0.22 and 0.8. Simultaneously, as the T-block's relative width grows, the transmission coefficient decreases. When b/B=0.4 and the wave period is 4s, the transmission coefficient is as low as 0.22, and the effect of wave elimination reaches 78%; when T=5s, the relative width of the T-block has the greatest gain effect on the transmission coefficient, and the effect of wave elimination is increased by about 15%. However, as the period grows, the gain in wave dissipation with an increase in the relative width of the T-block declines, and when the period approaches 8s, the difference in transmission coefficients between the four models is no longer significant. This is because increasing the width of the T-block increases the ratio between the width of the floating breakwater and the wavelength, which improves the effect of wave elimination. However, if the wavelength exceeds three times the width of the floating breakwater, the improvement in the wave attenuation performance from expanding the width of the T-shaped blocks is dramatically reduced. This phenomenon is consistent with the results of most prior studies; that is, when the wavelength exceeds three times the breakwater's characteristic width, the structural geometric parameters become saturated in terms of the ability to dissipate wave bypassing and reflecting energy, and it is difficult to achieve significant improvements in wave dissipation performance by increasing the width further.

To investigate the effect of the transmission coefficient on the incident wave height, a combined floating breakwater with T-block relative width b/B=0.4 was numerically simulated. The results are shown in Fig. 22 in the form of a bar chart to illustrate the change in transmission coefficient with incident wave height at the same water depth and period.

An analysis of Fig. 22 reveals that the variation in the amplitude of the transmittance coefficient with a change in wave height is modest. At different wave heights, the numerical value of the transmission coefficient for each period does not change a great deal, and it is only at T=8s that the transmission coefficient exhibits a rising trend as the wave height increases, although its numerical value does not change much. At the same time, it can be seen that the transmission coefficients at different wave heights all increase with the wave period, and that the upward trend is larger than for the change in wave height. A comprehensive analysis shows that the wave period is the most important wave parameter affecting the wave dissipation performance of the floating breakwater.

Fig. 22. Influence of different wave heights on the transmission coefficient

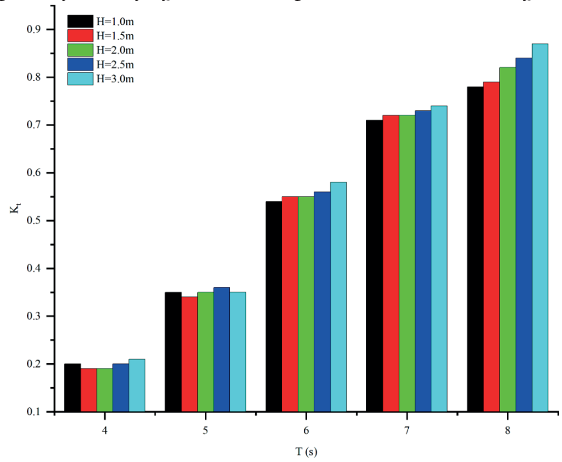

INFLUENCE OF BREAKWATER DRAFT ON WAVE DISSIPATION PERFORMANCE

To enable an analysis of the effect of the breakwater draft on wave dissipation performance, Figs. 23–27 show the variation in the transmission coefficients of the combined pontoon floating breakwater with different T-block widths at different draft depths, for wave heights of 1.0, 1.5, 2.0, 2.5, and 3.0 m, and periods of 4, 5, 6, 7, and 8s, respectively.

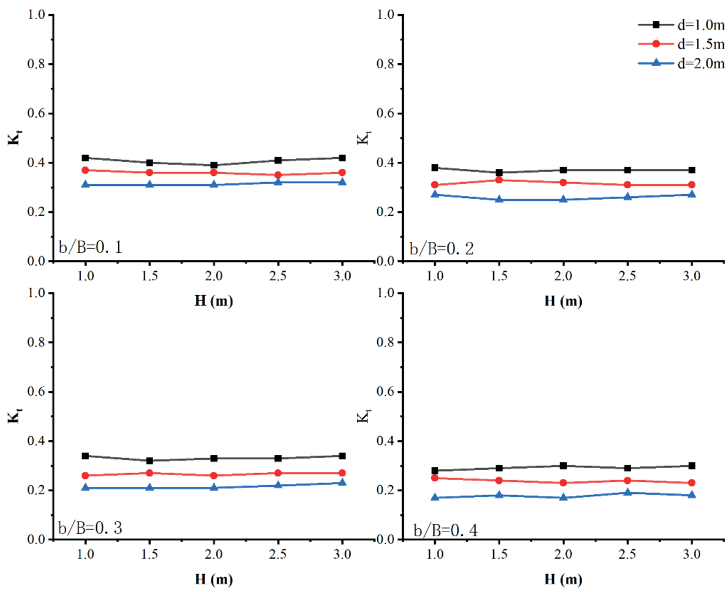

Fig. 23. Effect of different draft depths on transmission coefficient for T=4 s

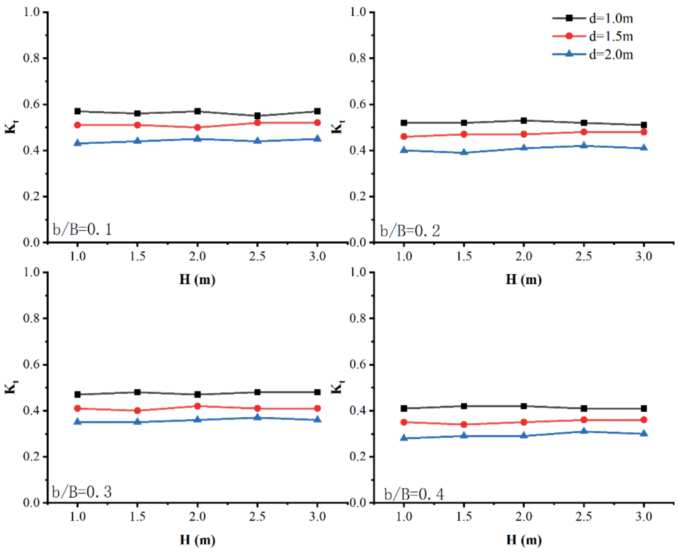

Fig. 24. Effect of different draft depths on transmission coefficient for T=5 s

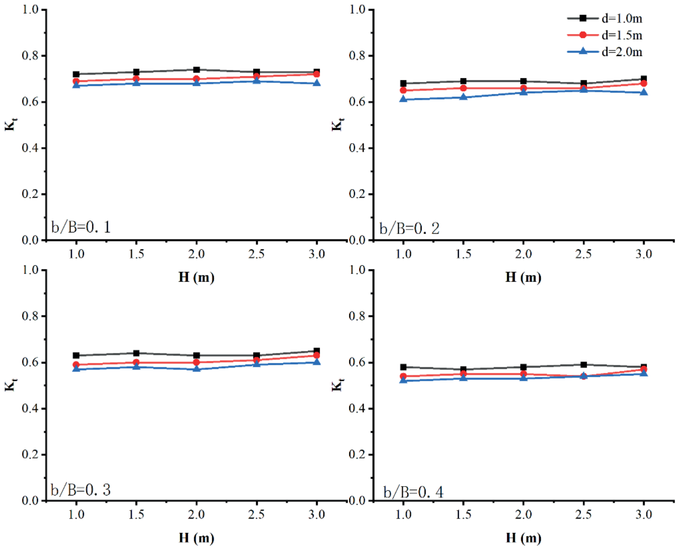

Fig. 25. Effect of different draft depths on transmission coefficient for T=6 s

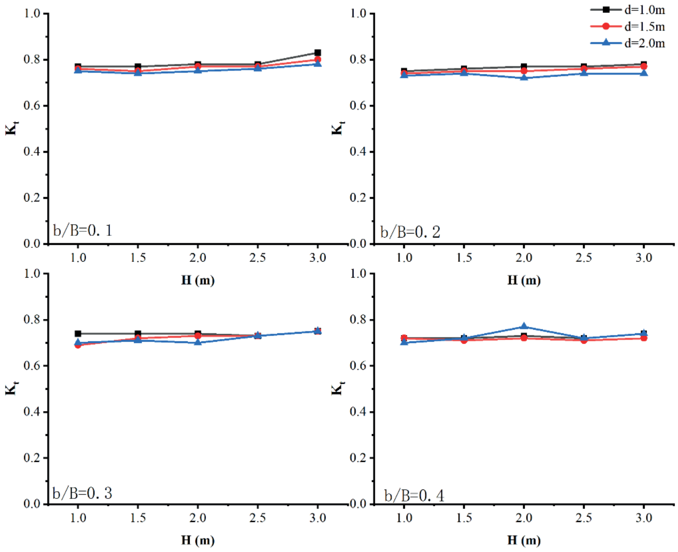

Fig. 26. Effect of different draft depths on transmission coefficient for T=7 s

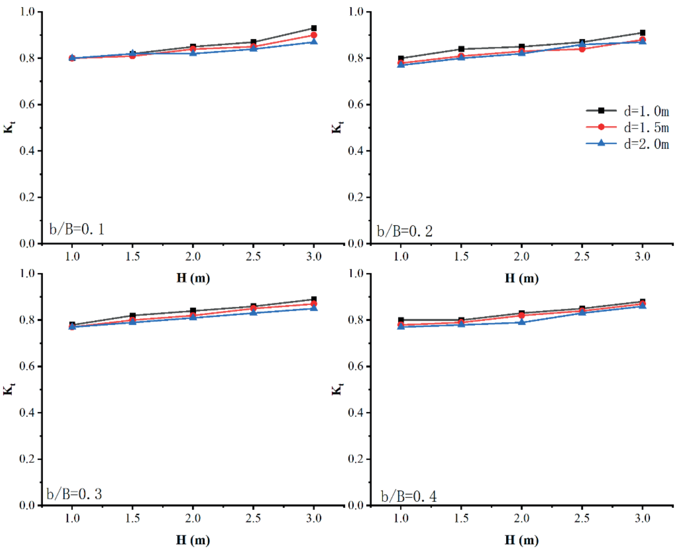

Fig. 27. Effect of different draft depths on transmission coefficient for T=8 s

The graphs in Figs. 23–27 demonstrate that when the wave period is modest, such as 4s, the influence of the structural draft on wave dissipation performance is substantial. Specifically, the wave removal effect shows a clear trend towards improvement with increasing draft depth. This is because the combined pontoon floating breakwater is a reflecting breakwater, resulting in a large wave energy attenuation effect primarily through the reflection of incident waves by the structure. However, as the wave period and wavelength rise, the wrap-around effect becomes increasingly important in the flow field. The water mass travels through the structure via wrap-around, which significantly reduces the effectiveness of the reflecting action. When the wave period exceeds 6s, the effect of wave elimination becomes less noticeable, whereas when the wave period exceeds 8s, an increase in the draft has almost no effect on the transmission coefficient, and the transmission coefficient gradually increases as the wave height increases.

COMPARISON OF WAVE ABATEMENT EFFECTS

A numerical simulation was conducted on a single pontoon-type floating breakwater with the same dimensions as the combined pontoon structure. Typical single-row and double-row pontoon configurations were analyzed under various draft depths and wave periods of 4 s, 5 s, 6 s, 7 s, and 8 s. The transmission coefficients under different conditions were obtained, and the corresponding wave attenuation performance was evaluated using the following equation. The Wave elimination effect is defined as:

$$\text{Effect of wave elimination} = (1 - K_t) \times 100\% \quad \textbf{(15)}$$

where K_t is the transmission coefficient.

Table 8 shows the wave elimination effect for pontoons arranged in a single row and for a composite breakwater with different draft depths (d). It also gives the performance gap between the composite and single-row pontoon floating breakwaters under identical wave periods. Fig. 28 displays a comparative diagram of the wave attenuation effects between typical single-row pontoons and a composite pontoon floating breakwater at d=1.0, 1.5, and 2.0 m.

Table 8. Comparison of wave elimination effect with a single-row pontoon breakwater

Draft	Period	Single row of pontoons	Combination of pontoons	Difference
1.0	4	52%	72%	20%
	5	26%	59%	33%
	6	19%	42%	23%
	7	19%	28%	9%
	8	16%	22%	6%
1.5	4	59%	78%	19%
	5	21%	65%	44%
	6	17%	44%	27%
	7	15%	28%	13%
	8	15%	22%	7%
2.0	4	65%	83%	18%
	5	35%	72%	37%
	6	22%	48%	26%
	7	21%	30%	9%
	8	20%	23%	3%

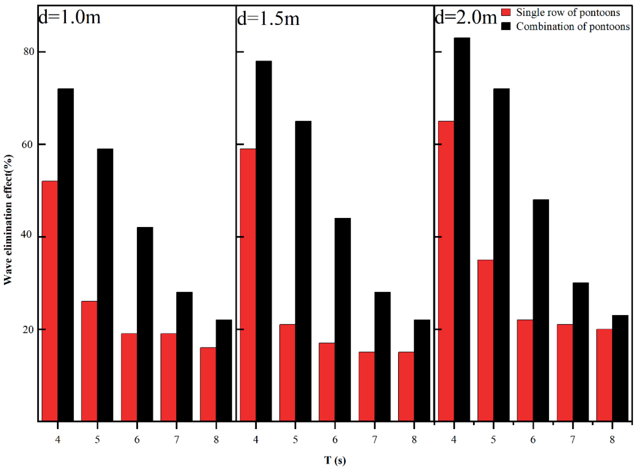

Fig. 28. Comparison of the wave elimination effect of single-row and composite pontoon breakwaters

From Table 8 and Fig. 28, it can be seen that the composite pontoon-type floating breakwater performs much better in terms of wave attenuation than the single-row version. Under a wave period of T=4s, the wave dissipation coefficient of this structure is improved by around 20% compared to the single-row arrangement at three draft depths (d=1.0, 1.5, and 2.0 m). When the wave period is increased to 5s, the wave attenuation performance reaches its maximum, with the magnitude of the improvement rising significantly to 37–44%. Notably, once the wave period exceeds 5s and above, the wave dissipation advantage of the composite breakwater rapidly fades. When T≥7s, the difference in the wave dissipation coefficients between the two structures drops to below 10%.

The study also demonstrates that the draft depth influences the wave dissipation performance. From the figure above, it is clear that the combined barge structure yields the best wave dissipation effect under intermediate draft conditions (d=1.5 m), and that the wave dissipation impact is greatly enhanced compared to the shallow draft (d=1.0 m) and deep draft (d=2.0 m) conditions. In particular, the wave dissipation effect is improved by 44% at T=5 s and d=1.5 m.

Table 9 compares the wave attenuation performance of a double-row pontoon configuration and a composite pontoon-type floating breakwater at a draft depth of d=2.0 m. It also shows the difference in the wave dissipation effectiveness between the composite configuration and a single-row of pontoons for identical wave periods. Fig. 29 compares the performance of the double-row pontoon arrangement and the composite pontoon-type floating breakwater at d=2.0 m, where the X-axis represents the wave period and the Y-axis shows the wave elimination effect.

Table 9. Comparison of wave elimination effect with a double-row pontoon breakwater

Type of breakwater	Period				
	4 s	5 s	6 s	7 s	8 s
Double row of pontoons	69%	41%	34%	25%	19%
Combined pontoon break-water	83%	72%	48%	30%	23%
Difference	14%	31%	14%	5%	4%

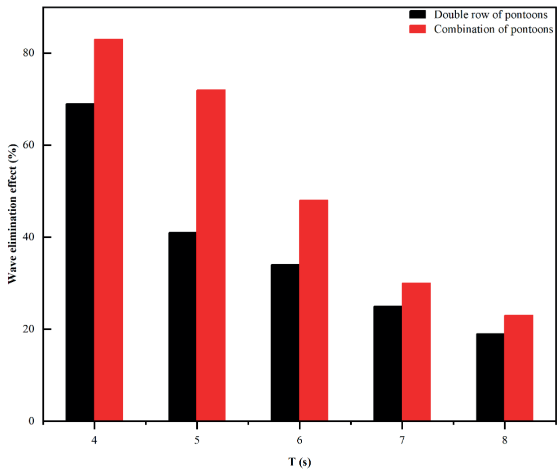

Fig. 29. Comparison with the wave elimination effect of single row of pontoons

An analysis of Table 9 and Fig. 29 shows that the combined pontoon floating breakwater gives a better wave elimination effect than the typical pontoon floating breakwater with a double row arrangement under different wave periods. When the draft is d=2.0 m, and especially when the period is T=5s, the advantage is most significant, with a difference of 31%. As the wave period increases, the difference in the wave elimination effect between a typical floating breakwater with a double row of pontoons and the combined pontoon floating breakwater gradually decreases, but the latter always maintains a relative advantage over the former in terms of wave elimination.

In summary, the floating breakwater based on a combination of pontoons offers substantial advantages in terms of wave removal. Compared to the single-row configuration of the breakwater, it yields good performance over a diverse range of wave periods and draft depths, and particularly at T≤6s. Compared to a normal pontoon floating breakwater, the wave elimination effect is superior for all values of the period at a given draft depth; however, this advantage declines as the period increases.

MOTION RESPONSE ANALYSIS

The stability of the floating breakwater must be considered in engineering applications to ensure safe operation . The free motion response of the floating breakwater is therefore studied here through numerical simulation. The motion response operator of the floating body, or RAO, is commonly used to express its free motion state in a frequency domain analysis. The RAO refers to the motion induced by a regular wave with unit amplitude, which is commonly expressed in terms of a response amplitude and phase, reflecting the relationship between the motion of the floating body and the frequency and direction of the wave.

Since the effect of waves on breakwater stability is particularly significant in regard to roll and heave motions, this study focuses on an analysis of the amplitude of motion in the roll and heave directions for the proposed breakwater in the presence of positive incident waves.

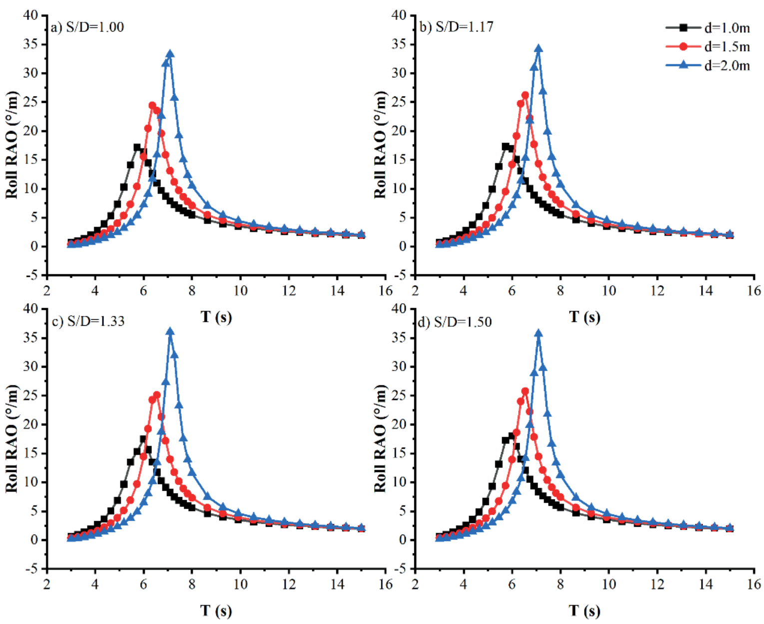

Fig. 30. Transverse rocking motion response for different draft depth conditions (relative height)

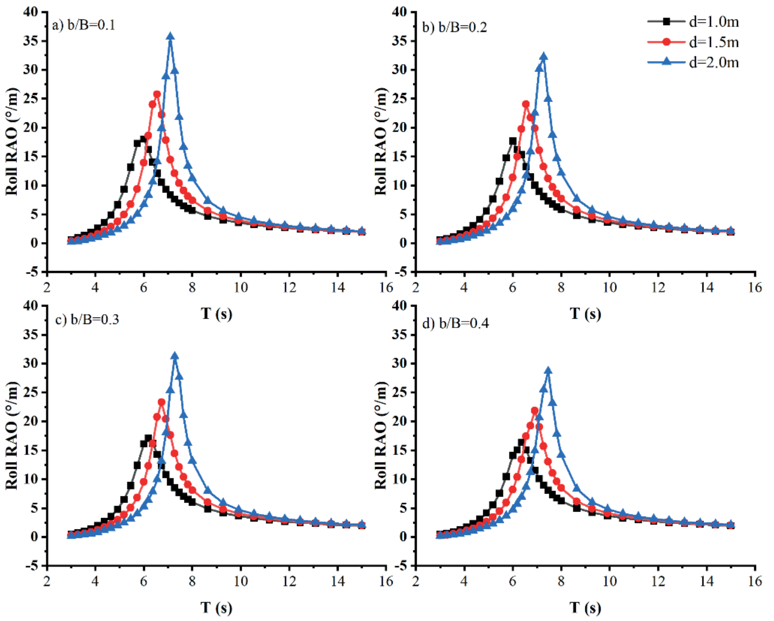

Fig. 31. Transverse rocking motion response for different draft depth conditions (relative width)

Figs. 30–33 depict the amplitude operators for the transverse roll response and the longitudinal roll response of the combined pontoon floating breakwater with various T-block combinations under varying draft conditions.

The following conclusions can be drawn from an evaluation of the response characteristics of a pontoon floating breakwater with varying relative heights of the T-block, as shown in Fig. 30. Under constant draft conditions, the transverse roll amplitude operator curves of the four types of models all display a single-peak distribution, and their motion patterns are very similar, as the amplitude increases with the wave cycle. The amplitude rises with the wave period, then drops quickly and stabilises. It is worth noting that under the same draft condition, the maximum roll amplitude does not greatly differ between the models.

A careful study reveals that as the draught depth rises from d=1.0 m to d=2.0 m, the model's centre of gravity moves downward, causing a shift in the system's intrinsic period. The experimental data show that when d=1.0 m, the maximum roll amplitude of 15°/m occurs at T=6.00s; when the draft is increased to d=1.5 m, the resonance period is delayed to T=6.54s, at which point the amplitude jumps to 25°/m; and when d=2.0 m, the system produces a violent roll response of more than 35°/m at T=7.09s. The amplitude of the roll motion increases sharply with the draft depth, exacerbating the instability of the breakwater in the direction of transverse roll.

It is evident from an analysis of the response characteristics of the transverse roll motion of the breakwater with varying relative widths of the T-block combination (Fig. 31) that the maximum transverse RAO of the structure undergoes a significant decrease for a given draft condition as the relative width of the T-block (b/B) is increased from 0.1 to 0.4, and the resonance corresponds to a systematic shift of the incident wave period. For a draft depth of d = 2.0 m, when b/B = 0.1, the system achieves a peak response of 35.69°/m at T = 7.09s.As b/B increases to 0.4, the maximum RAO decreases to 25.49°/m, with the corresponding wave period delayed to T = 7.45s, and the amplitude reduction reaching 10°/m.This suggests that increasing the width of the T-shaped blocks helps regulate the roll motion response of the combined floating breakwater.

A comparison with Fig. 30 reveals that the variation patterns under different draft conditions are closely aligned with the findings from the studies of the T-block height. As the draft depth is progressively increased from d=1.0 m to d=2.0 m, the roll RAO for all width-configured models undergoes consistent growth as the draft increases. This amplification effect leads to rapid deterioration in the stability of the breakwater in the roll direction, thereby reconfirming that an increase in draft depth substantially intensifies the instability of composite pontoon-type floating breakwaters in roll motion.

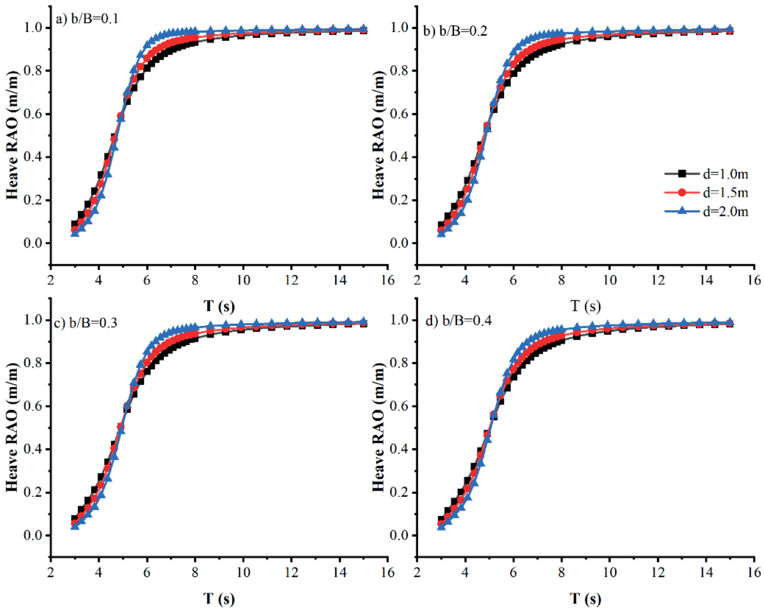

Fig. 33 Heave motion response for different draft depth conditions (relative width)

Fig. 32 shows the response of the breakwater composed of combined pontoons using T-blocks of different relative heights, with different draft depths. Fig. 33 shows the response of the proposed breakwater composed of combined pontoons using T-blocks with different relative widths, with different draft depths.From the analysis of the two figures, it is evident that combined pontoon floating breakwaters with varying T-block parameters show similar trends in heave motion response with respect to wave period under different draft conditions.The following conclusions are drawn.

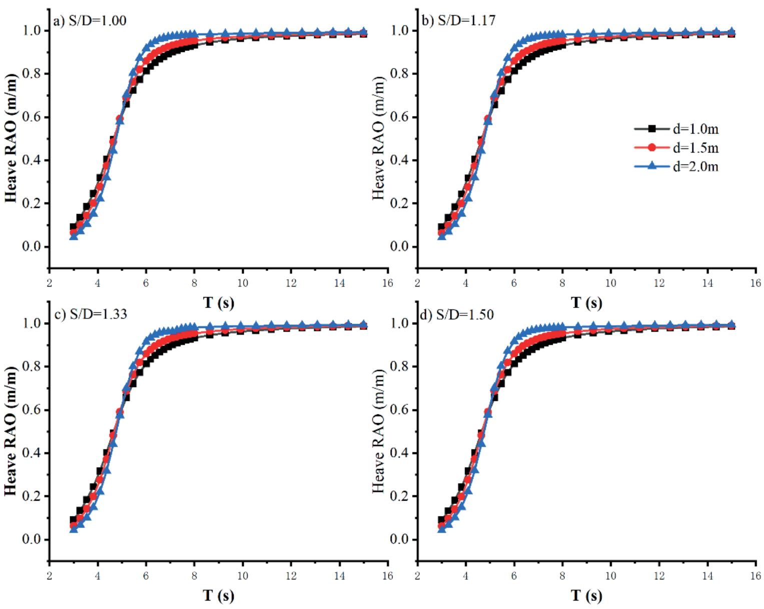

Fig. 32 Heave motion response for different draft depth conditions (relative height)

Changes in the relative height and breadth of the T-block or the draft depth of the structure have no significant influence on the direction of heave. The heave RAO tends to increase with the period, and the maximum magnitude of the breakwater's heave approaches a stable state when T>10 s. When combined with the RAO formula, it is clear that the maximum amplitude at this moment is equal to the maximum height of the incident wave. When the period of the incident wave is less than 5s, the heave RAO grows as the draft depth of the breakwater increases, but when T>5s, the heave RAO drops. It is worth noting that under a draft depth of d=1.5 m, the heave RAO remains consistently intermediate compared to the other two cases.

CONCLUSION

In order to improve the wave dissipation capacity of a typical pontoon floating breakwater, a combined floating breakwater including T-block connections has been designed and presented in this paper, and numerical simulations of its wave dissipation characteristics were carried out using AQWA software. The specific findings are as follows:

1. The combined pontoon floating breakwater significantly improves the wave dissipation capacity due to the T-block connection design. The wave elimination effect for a wave period of T≤6s is 20–44% higher than for a typical pontoon floating breakwater with single row arrangement, with the peak wave elimination effect (44% higher) observed at T=5s. Compared with a double-row arrangement, the combined structure maintains a significant advantage in terms of

the wave elimination effect at d=2.0 m, especially at T=5 s, when the difference reaches 31%.

2. The transmission coefficient of the combined floating breakwater increases with wave period. When the incident wave period is T<6s, increasing the relative height of the T-shaped blocks enhances the wave attenuation performance. However, for T>6s, the influence of T-block height on the transmission coefficient becomes weaker, and by T =8s, changes in height have almost no effect. Compared to variations in relative height, changes in the relative width of the T-blocks have a more significant impact on improving wave attenuation. As the relative width of the T-block increases, the transmission coefficient decreases. For example, at a draft of 1.0 m and incident wave height of 1.0 m with T=4s, the minimum transmission coefficient reaches 0.22. The greatest wave attenuation benefit from increasing the relative width occurs when the wave period is T=5s.
3. Compared to the incident wave period, the wave height has a less significant influence on the transmission coefficient of the composite floating breakwater. At identical wave periods, increasing the wave height induces minimal variation in the transmission coefficient, with a discernible upward trend observed only at T=8s as the wave height escalates.
4. When the wave period is small, e.g. 4s, the draft of the structure has a more obvious effect on the wave elimination performance; in other words, the wave elimination effect increases as the draft becomes larger. However, as the wave period increases (T>6s), the draft no longer has a significant effect on wave elimination.
5. A motion response analysis shows that the heave motion does not change significantly with an increase in the draught. The maximum peak value of the roll motion increases with the draft. The period corresponding to the maximum peak value of the roll also increases, which aggravates the instability of the breakwater in the direction of the roll, meaning that in a real-world project, a reasonable draught depth should be selected by considering the performance of the wave dissipation and the stability of the breakwater.

The combined pontoon floating breakwater proposed in this study can make effective use of abandoned pontoons, and can provide a cost-effective and efficient wave dissipation solution for port projects. Future research could focus on further optimising the geometric parameters of the T-block and the design of the mooring system, and exploring its adaptability under multi-directional irregular wave conditions in order to enhance the comprehensive protection capability under complex sea conditions.

REFERENCES

1. Shen YS, Zhou YR, Pan JN, Wang XG. Research progress on floating breakwaters. Journal of Hydraulic Engineering and Water Resources 2016, vol. 5, pp. 124-132. doi: https://doi.org/10.16198/j.cnki.1009-640X.2016.05.018
2. Ji CY, Cheng Y. Hydrodynamic and wave attenuation performance analysis theories and methods for floating breakwaters. Beijing: Science Press; 2018. ISBN 978-7-03-059330-6
3. Fu RU, Mao JZ, Yin WJ, Xu YB. Research status of floating breakwater structure. Port & Waterway Engineering 2016, vol. 6, pp. 61-66. https://doi.org/10.16233/j.cnki.issn1002-4972.2016.06.012
4. Dong HY. Study on hydrodynamic characteristics of a box-horizontal plate floating breakwater. PhD thesis, Dalian University of Technology, 2010.
5. Lianyungang Built China's First Floating Breakwater: Sea Surface Converted into "Fertile Land". Retrieved from: https://news.sina.com.cn/c/2002-09-03/1315704178.html
6. Sawaragi T. Coastal engineering—Waves, beaches, wave-structure interactions. Elsevier; 1995. ISBN 0-08-054484-3
7. Ji C-Y, Chen X, Cui J, Yuan Z-M, Incecik A. Experimental study of a new type of floating breakwater. Ocean Eng 2015, vol. 105, pp. 295-303. https://doi.org/10.1016/j.oceaneng.2015.06.046.
8. He CY, Wang DT, Feng WB. Study on wave attenuation performance of rectangular box-type floating breakwater. Port & Waterway Engineering 2014, vol. 1, pp. 14-18. https://doi.org/10.16233/j.cnki.issn1002-4972.2014.01.001
9. Loukogeorgaki E, Yagci O, Sedat Kabdasli M. 3D experimental investigation of the structural response and the effectiveness of a moored floating breakwater with flexibly connected modules. Coast Eng 2014, vol. 91, pp. 164-180. https://doi.org/10.1016/j.coastaleng.2014.05.008
10. Loukogeorgaki E, Lentsiou EN, Aksel M, Yagci O. Experimental investigation of the hydroelastic and the structural response of a moored pontoon-type modular floating breakwater with flexible connectors. Coast Eng 2017, vol. 121, pp. 240-254. https://doi.org/10.1016/j.coastaleng.2016.09.002.
11. Li S, Wei F, Xu H, Li Y, Zhang L. Experiment study on wave attenuation performance of a new type of porous floating breakwater. Ocean Eng 2024, vol. 309, p. 118334. https://doi.org/10.1016/j.oceaneng.2024.118334
12. Hou Y. Experimental study on hydrodynamic characteristics of single box-chain floating breakwater. Master's Thesis, Dalian University of Technology, 2009.
13. Cheng X, Li S, Wang G. Experimental study on hydrodynamic characteristics of barge-type breakwaters under different mooring methods. J Mar Sci Eng 2023, vol. 11, p. 1016. https://doi.org/10.3390/jmse11051016

14. Sutko AA. Floating breakwaters—A wave tank study. J Pet Technol 1975, vol. 27, pp. 269-273. https://doi.org/10.2118/4728-PA

15. Christian CD. Floating breakwaters for small boat marina protection. Proceedings of the Coastal Engineering 2000; American Society of Civil Engineers: Sydney, Australia, March 23 2001; pp. 2268-2277.

16. Headland JR, Vallianos L. Dynamic analysis of floating breakwater mooring systems. Proceedings of the Coastal Engineering 1990; American Society of Civil Engineers: Delft, The Netherlands, May 20 1991; pp. 1320-1333.

17. Chen C, Chen XQ, Yang Q, Lyu WY. Wave attenuation performance of wing-plate floating breakwater. Port & Waterway Engineering 2022, vol. 9, pp. 8-14+85. doi: https://doi.org/10.16233/j.cnki.issn1002-4972.20220901.024

18. Cheng X, Liu C, Zhang Q, He M, Gao X. Numerical study on the hydrodynamic characteristics of a double-row floating breakwater composed of a pontoon and an airbag. J Mar Sci Eng 2021, vol. 9, p. 983. https://doi.org/10.3390/jmse9090983

19. Wang G, Bar D, Schreier S. The potential of end-of-life ships as a floating seawall and the methodical use of gap resonance for wave attenuation. Ocean Eng 2024, vol. 298, p. 117246. https://doi.org/10.1016/j.oceaneng.2024.117246

20. Yin Z, Ni Z, Luan Y, Zhang X, Li J, Li Y. Hydrodynamic characteristics of a box-type floating breakwater with restrained piles under regular waves. Ocean Eng 2023, vol. 280, p. 114408. https://doi.org/10.1016/j.oceaneng.2023.114408

21. Tabatabaei SMR, Zeraatgar H. Parametric comparison of rectangular and circular pontoons performance as floating breakwater numerically. Pol Marit Res 2018, vol. 25, pp. 94-103. https://doi.org/10.2478/pomr-2018-0029

22. Zheng Y, Li J, Mu Y, Zhang Y, Huang S, Shao X. Numerical study on wave dissipation performance of OWC-perforated floating breakwater under irregular waves. Sustainability 2023, vol. 15, p. 11427. https://doi.org/10.3390/su151411427

23. Mao XQ, Guo JT, Ji CY, Bian XQ. Analysis of wave load characteristics for arc-layout floating breakwater. Ship Science and Technology 2022, vol. 44, pp. 92-99. https://doi.org/10.3404/j.issn.1672-7649.2022.15.019.

24. Wu S-X, Sun P-N, Li Q-Y, Rubinato M, Chen J-Q. Numerical study on a new floating breakwater with openings, arc-shaped wings, and plates using the SPH method. Ocean Eng 2025, vol. 324, p. 120353. https://doi.org/10.1016/j.oceaneng.2025.120353

25. Yuan H, Zhang H, Wang G, Tu J. A numerical study on a winglet floating breakwater: enhancing wave dissipation performance. Ocean Eng 2024, vol. 309, p. 118532. https://doi.org/10.1016/j.oceaneng.2024.118532

26. Sun B, Li C, Yang S, Zhang H, Song Z. Experimental and numerical study on the wave attenuation performance and dynamic response of kelp-box type floating breakwater. Ocean Eng 2022, vol. 263, p. 112374. https://doi.org/10.1016/j.oceaneng.2022.112374

27. Guo W, Zou J, He M, Mao H, Liu Y. Comparison of hydrodynamic performance of floating breakwater with taut, slack, and hybrid mooring systems: An SPH-based preliminary investigation. Ocean Eng 2022, vol. 258, p. 111818. https://doi.org/10.1016/j.oceaneng.2022.111818

28. Ursell F. The effect of a fixed vertical barrier on surface waves in deep water. Math Proc Camb Philos Soc 1947, vol. 43, pp. 374-382. https://doi.org/10.1017/S0305004100023604

29. eelamani S, Rajendran R. Wave interaction with T-type breakwaters. Ocean Eng 2002, vol. 29, pp. 151-175. https://doi.org/10.1016/S0029-8018(00)00060-3

30. Gesraha MR. Analysis of shaped floating breakwater in oblique waves: I. Impervious rigid wave boards. Appl Ocean Res 2006, vol. 28, pp. 327-338. https://doi.org/10.1016/j.apor.2007.01.002

31. Huang Z, He F, Zhang W. A floating box-type breakwater with slotted barriers. J Hydraul Res 2014, vol. 52, pp. 720-727. https://doi.org/10.1080/00221686.2014.888690

32. He F, Huang Z, Wing-Keung Law A. Hydrodynamic performance of a rectangular floating breakwater with and without pneumatic chambers: An experimental study. Ocean Eng 2012, vol. 51, pp. 16-27. https://doi.org/10.1016/j.oceaneng.2012.05.008

33. China Classification Society. Rules for Construction of Steel River Ships. 6th ed. Beijing, China: China Communications Press; 2016.

34. Wang SQ, Liang BC. Wave mechanics in ocean engineering. Qingdao, China: China Ocean University Press; 2013. ISBN 978-7-5670-0235-7